Conclusion

We encountered a case of PRES after UAE for uterine myoma. To the best of our knowledge, ours is the first report of this finding.

References

1. Hinchey J, Chaves C, Appignani B et al (1996) A reversible posterior leukoencephalopathy syndrome. N Engl J Med 334:494–500
2. Saigal G, Bhatia R, Bhatia S, Wakhloo AK et al (2004) MR findings of cortical blindness following cerebral angiography: is this entity related to posterior reversible leukoencephalopathy? Am J Neruroradiol 25:252–256
3. Tamaki K, Sadoshima S, Baumbach GL et al (1984) Evidence that disruption of blood-brain barrier precedes reduction in cerebral blood flow in hypertensive encephalopathy. Hypertension 6(2 Pt 2):I75–I81
4. Zoka C, Furci L, Ghilardi F et al (1986) Cyclosporine induced endothelial cell injury. Lab Invest 55:455–462
5. Bartynski WA (2008) Posterior reversible encephalopathy syndrome, Part 2: controversies surrounding pathophysiology of vasogenic edema. Am J Neuroradiol 29:1043–1049
6. Jackson A, Stewart G, Wood A et al (1995) Transient global amnesia and cortical blindness after vertebral angiography: further evidence for the role of arterial spasm. Am J Neuroradiol 16:955–959
7. Horwitz NH, Wener L (1974) Temporary cortical blindness following angiography. J Neurosurg 40:583–586
8. Waldron RL, Brian RN (1975) Effect of contrast media on the blood brain barrier: an electron microscopic study. Radiology 116:195–198
9. Lauren M, Brubaker J, Smith K, Lee YZ et al (2005) Hemodynamic and permeability changes in posterior reversible encephalopathy syndrome measured by dynamic susceptibility perfusion-weighted MR imaging. Am J Neruoradiol 26:825–830
10. Casey SO, Smapaio RC, Michel E et al (2000) Posterior reversible encephalopathy syndrome: utility of fluid-attenuated inversion recovery MR imaging in the detection of cortical and subcortical lesions. Am J Neuroradiol 21:1199–1206
11. Covarrubias DJ, Luetmer PH, Campeau NG (2002) Posterior reversible encephalopathy syndrome: prognostic utility of quantitative diffusion-weighted MR images. Am J Neuroradiol 23: 1038–1048
12. McKinney AM, Short J, Truwit CL (2007) Posterior reversible encephalopathy syndrome: incidence of atypical regions of involvement and imaging findings. Am J Radiol 189:904–912
13. Pelage KP, Le Fref O, Soyer P et al (2000) Fibroid-related menorrhagia: treatment with supreselective embolization of the uterine arteries and midterm follow-up. Radiology 215:428–431
14. Tetsuya K, Toshiyuki K, Kentaro A (2006) Long-term outcomes of uterine artery embolization using gelatin sponge particles alone for symptomatic fibroids. Am J Radiol 186:848–854
15. Seiyou M, Khaleque K, Michio K et al (2006) Differential infiltration of macrophages and prostaglandin production by different uterine leiomyomas. Hum Rep 21:2545–2554

Radiofrequency Ablation for the Treatment of Bone Metastases From Hepatocellular Carcinoma

Masataka Kashima[1]
Koichiro Yamakado[1]
Haruyuki Takaki[1]
Toshio Kaminou[2]
Noboru Tanigawa[3]
Atsuhiro Nakatsuka[1]
Kan Takeda[1]

OBJECTIVE. The objective of our study was to retrospectively evaluate the clinical utility of bone radiofrequency ablation in patients with bone metastases from hepatocellular carcinoma (HCC).

MATERIALS AND METHODS. At three institutions, 40 consecutive HCC patients with 54 bone metastases received radiofrequency ablation. The mean maximum diameter of the bone metastases was 4.8 ± 2.3 (SD) cm (range, 1.0–12.0 cm). The feasibility and safety of the procedure and the pain relief achieved from the procedure were reviewed. Technical success was defined as correct placement of the radiofrequency electrode into the tumor target and completion of the planned ablation protocol. Survival and prognostic factors were evaluated.

RESULTS. Technical success was 100%. No major complication occurred aside from transient nerve injury in one patient (2.5%, 1/40). Pain relief was achieved in all patients with painful bone metastases except one (96.6%, 28/29). The respective 1-, 2-, and 3-year survival rates were 34.2% (95% CI, 19.2–49.1), 19.9% (95% CI, 7.0–32.8), and 10.0% (95% CI, 0–20.2), with a median survival time of 7.1 months. Complete ablation of bone metastases, a single bone lesion, negative α-fetoprotein levels, and the absence of viable intrahepatic lesions were significant factors for a better prognosis. The median survival time was, respectively, 12.5 months in 16 patients with negative α-fetoprotein levels, 16.8 months in 12 patients with complete tumor ablation, 16.8 months in 16 patients with a single bone metastasis, and 21.9 months in 17 patients with no viable intrahepatic HCCs.

CONCLUSION. Bone radiofrequency ablation is a safe, useful, and feasible therapeutic option for relieving pain in patients with HCC bone metastases. Prognostic factors reported herein can facilitate stratification of patients with HCC bone metastases.

Keywords: bone metastases, hepatocellular carcinoma, oncologic imaging, prognosis, radiofrequency ablation

DOI:10.2214/AJR.09.2975

Received April 28, 2009; accepted after revision July 20, 2009.

[1]Department of Radiology, Mie University School of Medicine, 2-174 Edobashi, Tsu, Mie 514-8507, Japan. Address correspondence to K. Yamakado (yama@clin.medic.mie-u.ac.jp).

[2]Division of Radiology, Faculty of Medicine, Tottori University, Yonago, Tottori, Japan.

[3]Department of Radiology, Kansai Medical University, Moriguchi, Osaka, Japan.

AJR 2010; 194:536–541

0361–803X/10/1942–536

The incidence of extrahepatic metastases has been reported as 14–37% in patients with hepatocellular carcinomas (HCCs) [1]. Once metastasis occurs, patient survival is low [2, 3]: The 1-year survival rate is reportedly as low as 20.3–24.9%, with a median survival time of 4.6–7 months after systemic chemotherapy or external beam radiotherapy [3, 4].

Bones are reportedly the third most frequent site of distant metastases, after lungs and lymph nodes [3–8]. The incidence of bone metastases in HCC patients has been reported to be 6–20% in autopsy studies [5, 6] and 4–13% in clinical studies [7, 8].

External-beam radiotherapy is the standard palliative to relieve pain from bone metastases. Its effect on pain relief has been reported as 50–90% [9–11]. However, 12–20 weeks of therapy is required before pain relief occurs [11].

Radiofrequency ablation has proven to be a useful therapeutic option for the treatment of bone neoplasms. Its efficacy is not only in relieving pain in a shorter period but also in controlling tumors [12–17]. Some investigators have reported that control of extrahepatic metastases using surgical intervention, external-beam radiotherapy, and systemic chemotherapy prolonged survival in selected patients with HCCs [9, 18–23]. However, few previous reports have described the prognosis of patients with HCC bone metastases who have undergone bone radiofrequency ablation.

This retrospective multicenter study was conducted to evaluate the clinical utility of bone radiofrequency ablation in HCC patients with bone metastases.

Materials and Methods

Study Design

This retrospective study was conducted as a three-institution study. Written informed consent to perform bone radiofrequency ablation was obtained from all patients before bone radiofrequency ablation. The institutional review boards of the respective institutions required no approval for this retrospective study.

Patient and Tumor Characteristics

Patients with three or fewer HCC bone metastases were included in this study.

The exclusion criteria to perform bone radiofrequency ablation were as follows: a performance status of 4, according to the Eastern Cooperative Oncology Group [24]; a platelet count of less than 50,000/μL; an international normalized ratio of more than 1.5; and the presence of symptomatic spinal cord compression.

Between September 2002 and May 2008, bone metastases appeared in 96 patients with HCC. The initial treatments for bone metastases were radiotherapy in 66 patients (68.8%, 66/96), radiofrequency ablation in 25 patients (26.0%), and best supportive care in the other five patients (5.2%, 5/96). Of the 66 patients who received radiotherapy, 15 patients received bone radiofrequency ablation. Therefore, 40 patients (41.7%, 40/96) received bone radiofrequency ablation in total. Of these 40 patients, 29 received bone radiofrequency ablation for pain relief, and the other patients received it for tumor control.

The characteristics of the study patients, 33 men and seven women, are presented in Table 1. Their mean age was 65.7 ± 8.6 (SD) years (range, 44–84 years).

At the time of bone radiofrequency ablation, 54 HCC bone metastases were found: 26 bone lesions (48.1%, 26/54) in the vertebrae, nine (16.7%, 9/54) in the ribs, nine (16.7%, 9/54) in the iliac bone, and 10 (18.5%, 10/54) in other areas.

Pretreatment Workup

Before bone radiofrequency ablation, all patients underwent a routine physical examination, laboratory tests, and diagnostic imaging studies. The imaging studies included bone scintigraphy; chest, abdominal, and pelvic CT; and bone and brain MRI. The diagnoses of bone metastases were based on imaging findings, such as bone scintigraphy, CT, and MRI findings, in addition to clinical findings. Contrast-enhanced MRI studies were performed in all patients with bone lesions within 1 month before radiofrequency ablation. Bone biopsy was performed in 13 patients who had had uncertain diagnoses before bone radiofrequency ablation.

TABLE 1: Patient and Tumor Characteristics at Baseline

Variable	No. (%) of Patients (n = 40)
Patient characteristics	
Age (y)[a]	
≤ 65	19 (47.5)
> 65	21 (52.5)
Sex	
Male	33 (82.5)
Female	7 (17.5)
Cause of liver disease	
Hepatitis B or C virus	29 (72.5)
Others	11 (27.5)
Child-Pugh class	
A	28 (70.0)
B or C	12 (30.0)
Appearance of bone metastasis	
≤ 3 years	28 (70.0)
> 3 years	12 (30.0)
Tumor characteristics	
Maximum tumor diameter	
≤ 5 cm	15 (37.5)
> 5 cm	25 (62.5)
No. of bone tumors	
Single	16 (40.0)
Multiple (2 or 3)	24 (60.0)
Painful bone lesion	
Yes	29 (72.5)
No	11 (17.5)
Initial treatment of HCC	
Hepatectomy	14 (35.0)
Other	26 (65.0)
Intrahepatic tumors	
Controlled	17 (42.5)
Not controlled	23 (57.5)
Extraosseous metastasis	
Present	16 (40.0)
Absent	24 (60.0)
Arterial embolization for bone metastasis	
Yes	12 (30.0)
No	28 (70.0)
External beam radiotherapy	
Yes	15 (37.5)
No	25 (62.5)
Systemic chemotherapy	
Yes	5 (12.5)
No	35 (87.5)

(Table 1 continues on next page)

TABLE 1: Patient and Tumor Characteristics at Baseline (continued)

Variable	No. (%) of Patients (n = 40)
α-fetoprotein level	
Positive (> 28.5 ng/mL)	24 (60.0)
Negative (≤ 28.5 ng/mL)	16 (40.0)
Des-γ-carboxy prothrombin level	
Positive (> 40 mAU/mL)	33 (82.5)
Negative (≤ 40 mAU/mL)	7 (17.5)

[a]Mean ± SD = 65.7 ± 8.6 years.

Bone Radiofrequency Ablation

Bone radiofrequency ablation was performed on an inpatient basis with the patient under conscious sedation and using local anesthesia. Fentanyl citrate (Fentanest, Daiichi Sankyo) was used for analgesia, and 1% or 2% lidocaine hydrochloride (Xylocaine Polyamp, AstraZeneca International) was used for local anesthesia. Antibiotics (cefazolin sodium, Cefamezin, Astellas Pharma; or levofloxacin, Cravit, Daiichi-Sankyo Pharmaceuticals) were administered before bone radiofrequency ablation and for the first 2–3 days after the procedure. The radiofrequency ablation procedure was performed by one or two authors who had more than 10 years of experience as an interventional radiologist at each institution. An internally cooled electrode (Cool-tip, Valleylab) was used. Real-time CT fluoroscopy (X-Vigor or Asteion, Toshiba) was used to place the radiofrequency electrode directly into the tumor or through an 11-gauge bone biopsy needle (Bone Marrow Harvest Needle, Medical Device Technologies) according to the tumor size, shape, and location. Subsequently, radiofrequency ablation was performed in the Impedance Control mode.

In nine patients with bone metastases that were in the vertebral bodies and for whom the maximum tumor diameters were larger than 3 cm, cement was injected immediately after bone radiofrequency ablation to prevent subsequent bone fracture [14, 15].

Technical success was defined as correct placement of the radiofrequency electrode into the tumor target and completion of the planned ablation protocol. The technical success rate was calculated on the basis of the number of radiofrequency ablation sessions.

Complications

Major complications were assessed based on previously described guidelines of imaging-guided tumor ablation [25]. The definition of a major complication is an event that engenders substantial morbidity and disability, increases the level of care, or results in hospital admission or a substantially lengthened hospital stay. All other complications were considered minor.

Pain Relief

In terms of evaluation of pain relief, the visual analog scale (VAS) score [14–17] was used in 29 patients (72.5%, 29/40) with painful bone metastases. Patients were asked to rate their average pain over the past 1 week before and 1 week after bone radiofrequency ablation (0 = no pain, 10 = pain as bad as can be imagined). A decrease in the VAS score by 2 points or more was considered to be an effective reduction of pain.

Local recurrent pain was reviewed from medical records. An increased VAS score over the baseline value was considered to be a local recurrence of pain.

Therapeutic Response

Local therapeutic effects were evaluated using contrast-enhanced MRI performed within 1 week after radiofrequency ablation. Disappearance of tumor enhancement was considered to indicate tumor necrosis. The volumes of the entire tumor and of the necrotic tumor were measured by tracing them on contrast-enhanced MRI. The degree of local tumor necrosis was expressed as the ratio to the local tumor volume.

Survivals

All patients were followed up until death or December 31, 2008. The follow-up period was the time from the day of the initial bone radiofrequency ablation to the last follow-up visit or death from any cause.

Statistical Analysis

The mean VAS scores 1 week before and 1 week after bone radiofrequency ablation were compared using Wilcoxon's rank sum test.

Cumulative overall survival rates were generated according to the Kaplan-Meier method. To identify significant prognostic factors, patients were divided into two groups according to pretreatment variables (Table 1). Treatment results showing whether complete bone tumor ablation was achieved also were used as a variable. Survival rates were compared using the log-rank test. The stepwise regression model was used to identify independent prognostic factors. Data are expressed as means ± SD. A p value of less than 0.05 was inferred statistically significant. Statistical analyses were performed using commercially available software (SPSS version 15, SPSS).

Results

Feasibility

In all, 61 bone radiofrequency sessions were performed for 54 bone lesions. The radiofrequency electrodes were placed into all tumor targets and the planned ablation protocol was completed; therefore, the technical success rate was 100%.

Complications

There was no major complication except transient nerve injury in one patient (2.5%, 1/40) in whom the bone metastasis was in the fifth lumbar spinous process and had invaded the spinal canal. In this patient, leg paralysis and vesicorectal dysfunction occurred the day after bone radiofrequency ablation. These symptoms improved within 1 week after steroid administration.

Neither a minor complication nor death occurred in relation to bone radiofrequency ablation.

Pain Relief

The VAS score was reduced by 2 points or more 1 week after bone radiofrequency ablation in 28 of the 29 patients with painful bone metastases (96.6%, 28/29). A significant decrease was found in the mean VAS score from 6.1 ± 2.5 (SD) before bone radiofrequency ablation to 1.8 ± 1.7 ($p < 0.001$) after the procedure. Local recurrent pain was reported from 1.2 to 19.3 months after bone radiofrequency ablation (mean, 6.8 ± 5.7 months) by 14 patients (48.3%, 14/29).

Therapeutic Effects

The final local tumor necrosis ratios were 20.9–100%, and the mean local tumor necrosis ratio was 72.7 ± 22.7%. In 12 patients (30.0%, 12/40), bone tumor enhancement was eradicated completely.

Survival and Prognostic Factors

During the mean follow-up period of 11.9 ± 12.6 months (range, 0.8–66.0 months), 35 patients (87.5%, 35/40) died. The causes of death are presented in Table 2. Progression of intrahepatic lesions (57.1%, 20/35) was the most frequent cause of death.

The overall 1-, 2-, and 3-year survival rates were, respectively, 34.2% (95% CI,

TABLE 2: Causes of Death

Cause of Death	No. (%) of Patients
Cancer	28 (80.0)
Intrahepatic tumor progression	20 (57.1)
Brain metastasis	2 (5.7)
Lung metastases	1 (2.9)
Not specified	5 (14.3)
Hepatic failure	2 (5.7)
Gastrointestinal bleeding	2 (5.7)
Unknown	3 (8.6)
Total	35 (100)

19.2–49.1), 19.9% (95% CI, 7.0–32.8), and 10.0% (95% CI, 0–20.2), with a median survival time of 7.1 months (Fig. 1).

The stepwise regression model showed that the number of bone metastases (p < 0.01; odds ratio [OR], 3.1; 95% CI, 1.4–7.0), α-fetoprotein level (p < 0.01; OR, 3.9; 95% CI, 1.6–9.5), and control of intrahepatic lesions (p < 0.0001; OR, 8.7; 95% CI, 3.3–23.3) were identified as independent factors with a significant effect on prognosis (Figs. 2–4). In addition to these three factors identified through multivariate analyses, univariate analysis revealed complete bone ablation as a significant prognostic factor (Fig. 2).

The 3-year survival rates and median survival time were, respectively, 10.4% (95% CI, 0–45.6) and 16.8 months in 12 patients with complete bone ablation (Fig. 2), 19.8% (95% CI, 0–37.9) and 12.5 months in 16 patients with negative α-fetoprotein levels (Fig. 3), 20.1% (95% CI, 0–43.1) and 16.8 months in 16 patients with a single bone metastasis (Fig. 4), and 24.5% (95% CI, 1.1–47.5) and 21.9 months in 17 patients with controlled intrahepatic lesions (Fig. 5). The other pretreatment baseline variables were not prognostic factors.

Discussion

The appearance of bone metastasis is a poor prognostic sign in patients with HCCs. The median or mean survival time of patients with bone metastasis has been reported to be 2.9 months with no treatment, 5 months after cementoplasty, and 6 months after external-beam radiotherapy [9, 15, 26]. In our study, the median survival time was almost identical to that of previous reports [3, 4, 9, 15, 26].

A controversy has arisen about whether treatment of bone metastases improves patient survival. Okusaka et al. [3] reported that most patients (90%, 9/10) with HCC bone metastasis die of hepatic causes—not the bone metastasis—and underscored the importance of controlling intrahepatic tumors. The results of our study also support their assertion with a larger patient series. More than half of the patients in our study died of intrahepatic tumor progression. Control of intrahepatic tumors was identified as a prognostic factor.

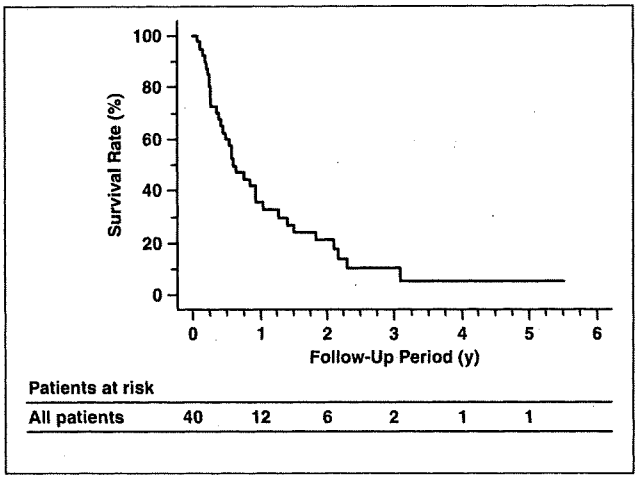

Fig. 1—Graph shows cumulative overall survival rate in 40 patients with hepatocellular carcinoma bone metastases after bone radiofrequency ablation. Overall 1-, 2-, and 3-year survival rates were, respectively, 34.2% (95% CI, 19.2–49.1), 19.9% (95% CI, 7.0–32.8), and 10.0% (95% CI, 0–20.2), with median survival time of 7.1 months.

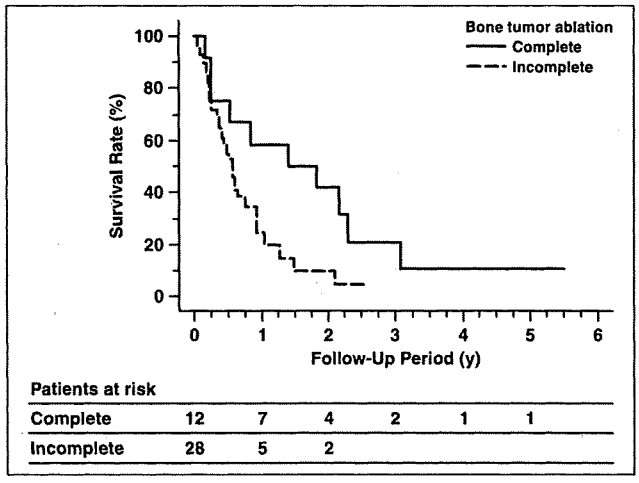

Fig. 2—Graph shows cumulative survival based on results of bone tumor ablation. Three-year survival rates and median survival time were 10.4% (95% CI, 0–45.6) and 16.8 months in 12 patients with complete tumor ablation and 0% and 6.5 months in 28 patients with incomplete tumor ablation (p < 0.04).

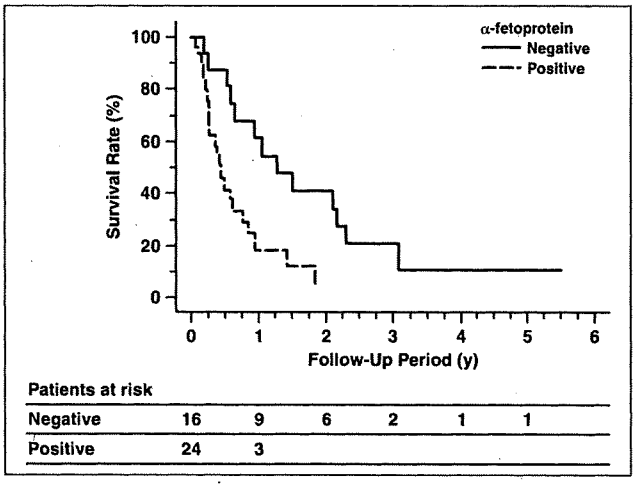

Fig. 3—Graph shows cumulative survival rates based on serum α-fetoprotein level. Three-year survival rates and median survival time were 19.8% (95% CI, 0–37.9) and 12.5 months in 16 patients with negative α-fetoprotein level and 0% and 5.0 months in 24 patients with positive α-fetoprotein level (p < 0.01).

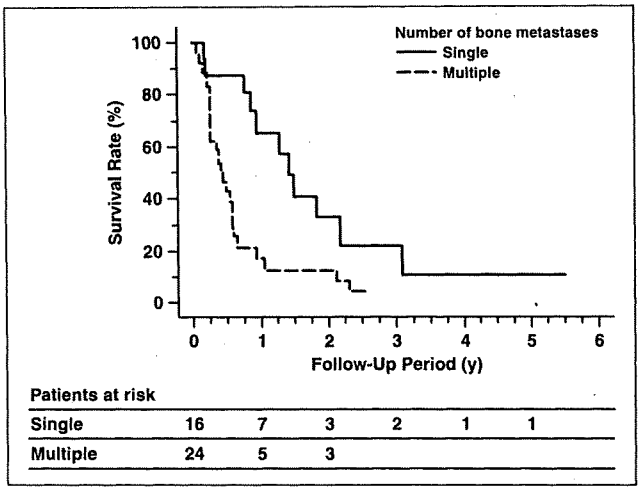

Fig. 4—Graph shows cumulative survival rates based on number of bone metastases. Three-year survival rates and median survival time were 20.1% (95% CI, 0–43.1) and 16.8 months in 16 patients with single bone metastasis and 0% and 5.0 months in 24 patients with multiple bone metastases ($p < 0.01$).

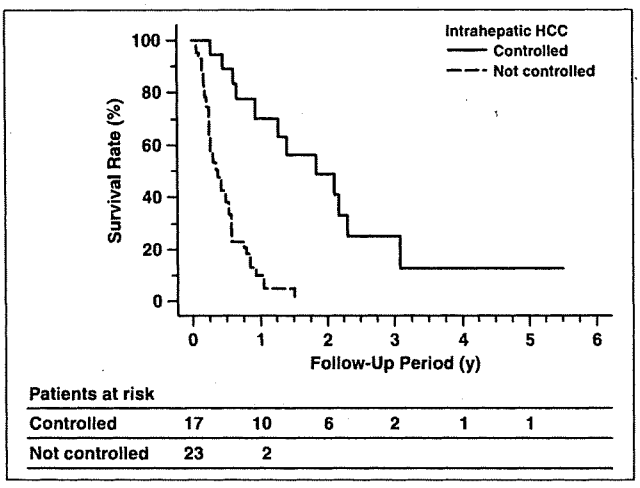

Fig. 5—Graph shows cumulative survival rates based on control of intrahepatic hepatocellular carcinoma (HCC). Three-year survival rates and median survival time were 24.5% (95% CI, 1.1–47.5) and 21.9 months in 17 patients with no viable (controlled) intrahepatic lesions and 0% and 4.4 months in 23 patients with viable (not controlled) intrahepatic lesions ($p < 0.0001$).

Other than control of intrahepatic tumors, the number of bone metastases and the serum α-fetoprotein level were identified as prognostic factors. The serum α-fetoprotein level reflects prognosis in patients with HCC [27]. Patients with a high α-fetoprotein concentration tend to have aggressive tumors that are large; bilobar involvement, massive or diffuse type; portal vein thrombosis; and a lower median survival rate [27].

Kaizu et al. [9] also reported that a single bone metastasis is a better prognostic factor in HCC bone metastasis patients who received external beam radiotherapy. These three factors seem to indicate that prognosis depends on tumor aggressiveness at the time of bone metastasis.

On the other hand, complete bone tumor ablation was identified as a better prognostic factor in univariate analysis. Some studies have emphasized the importance of controlling extrahepatic metastases to prolong survival in patients with HCCs [9, 18–23]. Our study showed the possibility that bone radiofrequency ablation can be part of a multidisciplinary treatment to control extrahepatic metastases and prolong patients' survival. In addition, our study shows the difficulty in achieving complete bone tumor ablation. Complete bone tumor ablation was achieved in only 30% (12/40) of the patients. Moreover, tumor multiplicity, large tumor size, and tumor location make it difficult to achieve complete tumor ablation. Difficulty in achieving complete bone tumor necrosis also seems to contribute to the high recurrence rate of pain. Whether bone radiofrequency ablation contributes to patient survival or not should be confirmed using larger patient series in future clinical trials.

Our results show that bone radiofrequency ablation is a safe and feasible therapeutic option for the treatment of HCC bone metastases. The complication rate after bone radiofrequency ablation was similar to those reported in previous reports in cancer of many types [12–17]. One patient (2.5%, 1/40) in our study experienced transient nerve injury; in that patient, the bone metastasis was in the lumbar spine. A risk of spinal nerve injury exists by radiofrequency ablation when the spinal canal wall is destroyed by the vertebral bone tumor [28]. It is useful to place a thermocouple in the spinal canal for monitoring the temperature of tissues adjacent to the nerve [13].

Our study was limited by its retrospective nature. However, as we described, our results can serve as a scaffold with which to design future clinical trials.

In conclusion, bone radiofrequency ablation is a safe, useful, and feasible therapeutic option for relieving pain in patients with HCC bone metastases. Prognostic factors identified in our study will help to stratify patients with HCC bone metastases.

References

1. Katyal S, Oliver JH 3rd, Peterson MS, Ferris JV, Carr BS, Baron RL. Extrahepatic metastases of hepatocellular carcinoma. *Radiology* 2000; 216: 698–703
2. Aramaki M, Kawano K, Kai T, et al. Treatment for extrahepatic metastasis of hepatocellular carcinoma following successful hepatic resection. *Hepatogastroenterology* 1999; 46:2931–2934
3. Okusaka T, Okada S, Ishii H, et al. Prognosis of hepatocellular carcinoma patients with extrahepatic metastases. *Hepatogastroenterology* 1997; 44:251–257
4. Natsuizaka M, Omura T, Akaike T, et al. Clinical features of hepatocellular carcinoma with extrahepatic metastases. *J Gastroenterol Hepatol* 2005; 20:1781–1787
5. Nakashima T, Okuda K, Kojiro M, et al. Pathology of hepatocellular carcinoma in Japan: 232 consecutive cases autopsied in ten years. *Cancer* 1983; 51:863–877
6. Yuki K, Hirohashi S, Sakamoto M, et al. Growth and spread of hepatocellular carcinoma: a review of 240 consecutive autopsy cases. *Cancer* 1990; 66:2174–2179
7. Taki Y, Yamaoka Y, Takayasu T, et al. Bone metastases of hepatocellular carcinoma after liver resection. *J Surg Oncol* 1992; 50:12–18
8. Fukutomi M, Yokota M, Chuman H, et al. Increased incidence of bone metastases in hepatocellular carcinoma. *Eur J Gastroenterol Hepatol* 2001; 13:1083–1088
9. Kaizu T, Karasawa K, Tanaka Y, et al. Radiotherapy for osseous metastases from hepatocellular carcinoma: a retrospective study of 57 patients. *Am J Gastroenterol* 1998; 93:2167–2171
10. Roca EL, Okazaki N, Okada S, et al. Radiotherapy for bone metastases of hepatocellular carcinoma. *Jpn J Clin Oncol* 1992; 22:113–116

11. Janian NA. Radiation for bone metastases: conventional techniques and the role of systemic radiopharmaceuticals. *Cancer* 1997; 80[8 suppl]:1628–1645
12. Callstrom MP, Charboneau JW, Goetz MP, et al. Painful metastases involving bone: feasibility of percutaneous CT- and US-guided radio-frequency ablation. *Radiology* 2002; 224:87–97
13. Nakatsuka A, Yamakado K, Takaki H, et al. Percutaneous radiofrequency ablation of painful spinal tumors adjacent to the spinal cord with real-time monitoring of spinal canal temperature: a prospective study. *Cardiovasc Intervent Radiol* 2009; 32:70–75
14. Nakatsuka A, Yamakado K, Maeda M, et al. Radiofrequency ablation combined with bone cement injection for the treatment of bone malignancies. *J Vasc Interv Radiol* 2004; 15:707–712
15. Kodama H, Aikata H, Uka K, et al. Efficacy of percutaneous cementoplasty for bone metastasis from hepatocellular carcinoma. *Oncology* 2007; 72:285–292
16. Kojima H, Tanigawa N, Kariya S, et al. Clinical assessment of percutaneous radiofrequency ablation for painful metastatic bone tumors. *Cardiovasc Intervent Radiol* 2006; 29:1022–1026
17. Grönemeyer DH, Schirp S, Gevargez A. Image-guided radiofrequency ablation of spinal tumors: preliminary experience with an expandable array electrode. *Cancer J* 2002; 8:33–39
18. Tanaka K, Shimada H, Matsuo K, et al. Clinical features of hepatocellular carcinoma developing extrahepatic recurrences after curative resection. *World J Surg* 2008; 32:1738–1747
19. Lo CM, Lai EC, Fan ST, et al. Resection for extrahepatic recurrence of hepatocellular carcinoma. *Br J Surg* 1994; 81:1019–1021
20. Shimada M, Takenaka K, Gion T, et al. Prognosis of recurrent hepatocellular carcinoma: a 10-year surgical experience in Japan. *Gastroenterology* 1996; 111:720–726
21. Yang Y, Nagano H, Ota H, et al. Patterns and clinicopathologic features of extrahepatic recurrence of hepatocellular carcinoma after curative resection. *Surgery* 2007; 141:196–202
22. Poon RT, Fan ST, O'Sulleabhain CB, et al. Aggressive management of patients with extrahepatic and intrahepatic recurrences of hepatocellular carcinoma by combined resection and locoregional therapy. *J Am Coll Surg* 2002; 195: 311–318
23. Ono T, Yamanoi A, Nazmy El Assal O, Kohno H, Nagasue N. Adjuvant chemotherapy after resection of hepatocellular carcinoma causes deterioration of long-term prognosis in cirrhotic patients: metaanalysis of three randomized controlled trials. *Cancer* 2001; 91:2378–2385
24. Oken MM, Creech RH, Tormey DC, et al. Toxicity and response criteria of the Eastern Cooperative Oncology Group. *Am J Clin Oncol* 1982; 5: 649–655
25. Goldberg SN, Grassi CJ, Cardella JF, et al.; Society of Interventional Radiology Technology Assessment Committee; International Working Group on Image-Guided Tumor Ablation. Image-guided tumor ablation: standardization of terminology and reporting criteria. *Radiology* 2005; 235:728–739
26. Kim SU, Kim do Y, Park JY, et al. Hepatocellular carcinoma presenting with bone metastasis: clinical characteristics and prognostic factors. *J Cancer Res Clin Oncol* 2008; 134:1377–1384
27. Zhou L, Liu J, Luo F. Serum tumor markers for detection of hepatocellular carcinoma. *World J Gastroenterol* 2006; 12:1175–1181
28. Adachi A, Kaminou T, Ogawa T, et al. Heat distribution in the spinal canal during radiofrequency ablation for vertebral lesions: study in swine. *Radiology* 2008; 247:374–380

Cement Leakage in Percutaneous Vertebroplasty for Osteoporotic Compression Fractures With or Without Intravertebral Clefts

Noboru Tanigawa[1]
Shuji Kariya[1]
Atsushi Komemushi[2]
Takanori Tokuda[1]
Miyuki Nakatani[1]
Rie Yagi[1]
Satoshi Sawada[1]

OBJECTIVE. The purpose of our study was to compare the incidence and location of cement leakage in percutaneous vertebroplasty for osteoporotic compression fractures with and without intravertebral clefts.

MATERIALS AND METHODS. Percutaneous vertebroplasty was performed in 120 consecutive patients with 300 osteoporotic compression fractures. The cement volume injected was recorded. The cement leakage was evaluated using spinal radiography, MRI, and fluoroscopy during the procedure and CT after the procedure.

RESULTS. One hundred seven vertebrae contained intervertebral clefts, and 193 vertebrae had no clefts. The cement volume injected (± SD) was 4.0 ± 2.0 and 3.6 ± 1.6 mL into vertebrae with clefts and without clefts, respectively, with no statistically significant difference ($p = 0.14$). There was no statistically significant difference in the incidence of cement leakage between vertebrae with clefts (53 of 107) and those without clefts (78 of 193) ($p = 0.13$). Leakage occurred into the epidural veins (12 of 107), perivertebral soft tissues (7 of 107), disks (41 of 107), intervertebral foramen (1 of 107), and spinal canal (1 of 107) in fractures with clefts and into the epidural veins (47 of 193), perivertebral soft tissues (13 of 193), disks (25 of 193), paravertebral veins (5 of 193), large vein (2 of 193), lung (2 of 193), intervertebral foramen (1 of 193), and spinal canal (1 of 193) in fractures without clefts. Cement leakage into the epidural vein was significantly more frequent in vertebrae without clefts ($p < 0.01$). Disk leakage was significantly more frequent in vertebrae with clefts compared with those without clefts ($p < 0.01$).

CONCLUSION. There was no statistically significant difference in the incidence of cement leakage between vertebrae with clefts and without clefts. However, cement leakage into the epidural vein was significantly more frequent in vertebrae without clefts and disk leakage was significantly more frequent in vertebrae with clefts.

Keywords: cement leakage, clefts, osteoporosis, vertebroplasty

DOI:10.2214/AJR.09.2774

Received March 20, 2009; accepted after revision May 11, 2009.

[1]Department of Radiology, Kansai Medical University, Hirakata Hospital, 2-3-1 Shinmachi, Hirakata, Osaka, 573-1191, Japan. Address correspondence to N. Tanigawa (tanigano@hirakata.kmu.ac.jp).

[2]Department of Radiology, Kansai Medical University, Takii Hospital, Moriguchi, Osaka, Japan.

WEB
This is a Web exclusive article.

AJR 2009; 193:W442–W445

0361–803X/09/1935–W442

The intravertebral cleft is generally considered a radiographic sign of avascular necrosis of the vertebral body associated with impairment of the vertebral blood supply and cartilaginous nodes and normal stress placed on a weakened vertebra [1–3]. This sign is highly suggestive of osteonecrosis, although it is not specific [4] and has not been described in association with acute vertebral fractures [5]. In other words, clefts are thought to represent fracture nonunion [1, 2].

In percutaneous vertebroplasty, the existence of clefts inside fractured vertebral bodies is significant, and back pain disappears by injecting cement into clefts to relieve instability in the fractured vertebrae [6–12]. Reports have indicated that cement can be injected easily into clefts at low pressure with minimal cement leakage outside the vertebral body [13]. In addition, kyphoplasty is a technique that prepares a gap, or cleft, in a fractured vertebral body using a balloon and then cement is injected. Compared with vertebroplasty, the degree of cement leakage outside the vertebra is lower for kyphoplasty [14, 15]. However, while the cement is being injected into a cleft during percutaneous vertebroplasty, cement sometimes leaks into the intervertebral disk connected to the cleft.

Leakage into the intervertebral disk is often asymptomatic but has been reported as one cause of new compression fractures after percutaneous vertebroplasty [14, 16, 17], and therefore leakage must be minimized. The purpose of this study was to compare the incidence and location of cement leakage in percutaneous vertebroplasty for osteoporotic compression fractures with and without intravertebral clefts.

Materials and Methods

This study was conducted on 120 consecutive patients (107 women, 13 men) with painful osteoporotic compression fractures treated using percutaneous vertebroplasty. The mean patient age was 73 years (age range, 44–86 years). A total of 300 vertebral bodies were treated. Locations and numbers of treated vertebral bodies were as follows: T5, $n = 2$; T6, $n = 5$; T7, $n = 7$; T8, $n = 13$; T9, $n = 11$; T10, $n = 11$; T11, $n = 23$; T12, $n = 50$; L1, $n = 63$; L2, $n = 34$; L3, $n = 43$; L4, $n = 23$; and L5, $n = 15$.

The indication for percutaneous vertebroplasty was back pain caused by vertebral body compression fracture, with pain on percussion of the vertebral spinous process. In cases with multiple compression fractures in which percussion pain of the spinous process was unclear, physical examination was performed using fluoroscopy. Patients with back pain attributed to myelopathy or radiculopathy resulting from stenosis of the vertebral canal or narrowing of the intervertebral foramen were excluded.

Percutaneous Vertebroplasty Procedure

Informed consent was obtained from all patients before the procedure. All procedures were performed by one of the authors who had 9 years of experience in percutaneous vertebroplasty or by a fellowship trainee under the supervision of the author. Percutaneous vertebroplasty was performed under combined CT and fluoroscopic guidance (Advantx LCA plus ACT, GE Healthcare). Thirty minutes preoperatively, 10 mg of morphine hydrochloride, 0.5 mg atropine sulfate, and 25 mg hydroxyzine hydrochloride were administered intramuscularly. Local anesthesia with 10 mL of 1% lidocaine was administered from the skin to the periosteum of the pedicle using a 22-gauge Cathelin needle (Terumo Europe) under fluoroscopic guidance. After orientation of the puncture needle was confirmed on CT and aligned with the Cathelin needle, a 13-gauge bone biopsy needle (Osteo-Site Bone Biopsy Needle Murphy M2, Cook) was advanced into the pedicle of the vertebral arch. A unilateral transpedicular approach was chosen in all cases. CT was repeated, and after the orientation of the biopsy needle was confirmed, the visualization technique was changed to lateral fluoroscopy and the bone biopsy needle was advanced to the anterior third of the vertebral body close to the midline.

Intraosseous venography was performed with 1–5 mL of iopamidol (Iopamiron 300, Schering Japan) or 5–20 mL of carbon dioxide to confirm that the needle was not positioned within a direct venous anastomosis to the central or epidural veins. Subsequently, 20 g of methylmethacrylate powder (Osteobond Copolymer Bone Cement, Zimmer) was mixed with 5 g of barium sulfate powder that had been sterilized with dry heat to increase its opacity. Next, 10 mL of liquid methylmethacrylate monomer was added to the powder, and the mixture was blended to a toothpastelike consistency, producing polymethylmethacrylate (PMMA). Using 1-mL syringes, the PMMA was injected with lateral fluoroscopic guidance. PMMA injection was terminated when adequate filling of the vertebral body was achieved or if leakage occurred. When a fractured cleft was filled with cement for the cases with clefts, we stopped the cement injection. The needle was then removed, and all patients were observed in the supine position for 2 hours.

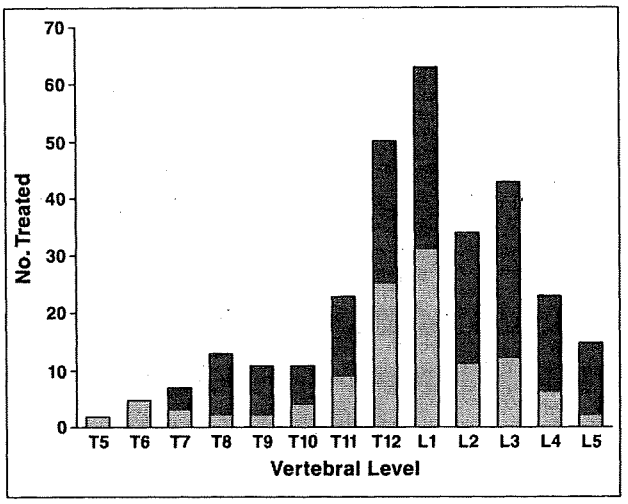

Fig. 1—Graph shows distribution of treated vertebral fractures. Light gray shading indicates without intravertebral clefts and dark gray shading indicates with intravertebral clefts.

Cleft and Leakage Diagnosis

Clefts were diagnosed on the basis of linear well-demarcated radiolucency inside a fractured vertebral body on preoperative radiography or, alternatively, using transverse signal hyperintensities on fat-suppressed T2-weighted MRI. Furthermore, linear well-demarcated radiolucency seen by intraoperative fluoroscopy and lesions in which cement was injected as compact and solid cement filling during PMMA injection were diagnosed as clefts. In addition, CT was performed immediately after PMMA injection, and compact and solid cement fillings also were diagnosed as clefts. Leakage outside vertebral bodies was assessed by CT immediately after PMMA injection, and 3D images were prepared to diagnose leakage location. Images including spinal radiography, MRI, and CT were evaluated by two of the authors who reached a consensus for each case. Chest radiographs were obtained to detect pulmonary cement embolism 1 day after percutaneous vertebroplasty. When a pulmonary cement embolism was suspected during the procedure, chest CT was performed immediately after the procedure.

Statistical Analysis

The volume of cement injection per vertebra was compared between vertebral bodies with and without clefts and analyzed using the Wilcoxon's rank-sum test. The chi-square test was used to compare occurrence rates of cement leakage.

TABLE 1: Cement Leakage Outside Vertebra With or Without Cleft

Location	With Cleft ($n = 107$)	Without Cleft ($n = 193$)	p
Epidural vein	12 (11.2)	47 (24.4)	> 0.01
Perivertebral soft tissue	7 (6.5)	13 (6.7)	0.95
Intervertebral disk	41 (38.3)	25 (13.0)	> 0.01
Paravertebral vein	0 (0)	5 (2.6)	0.09
Large vein[a]	0 (0)	2 (1.0)	0.29
Lung	0 (0)	2 (1.0)	0.29
Intervertebral foramen	1 (0.9)	1 (0.5)	0.67
Spinal canal	1 (0.9)	1 (0.5)	0.67
Total	62 (57.9)	96 (49.7)	

Note—Data are number of patients, and numbers in parentheses are percentages.
[a]Mean inferior vena cava and azygos vein.

All statistical analyses were conducted using StatView for Windows version 5.0 software (SAS Institute), and values of $p < 0.05$ were considered statistically significant.

Results

One hundred seven vertebrae contained intervertebral clefts, and 193 vertebrae had no clefts. Forty-three (40.2%) and 71 (66.4%) of 107 clefts were detected on spine radiography and MRI, respectively. On the other hand, 36 of 107 clefts (33.6%) were diagnosed on fluoroscopy during the procedure or on CT after the procedure. Locations of each vertebra are shown in Figure 1.

The mean volume of cement injected (± SD) was 4.0 ± 2.0 mL for vertebrae with clefts and 3.6 ± 1.6 mL for vertebrae without clefts, and the volumes were not significantly different ($p = 0.14$). There was no statistically significant difference in the incidence of cement leakage between vertebrae with clefts (53 of 107 vertebrae, 49.5%) and those without clefts (78 of 193 vertebrae, 40.4%) ($p = 0.13$). Leakage locations included the epidural vein (12 of 107, 11.2%), perivertebral soft tissue (7 of 107, 6.5%), intervertebral disk (41 of 107, 38.3%) (Fig. 2), intervertebral foramen (1 of 107, 0.9%), and spinal canal (1 of 107, 0.9%) in fractures with clefts; and the epidural vein (47 of 193, 24.4%) (Fig. 3), perivertebral soft tissues (13 of 193, 6.7%), intervertebral disk (25 of 193, 13.0%), paravertebral vein (5 of 193, 2.6%), large veins including the inferior vena cava and azygos vein (2 of 193, 1%), lung (2 of 193, 1%), intervertebral foramen (1 of 193, 0.5%), and spinal canal (1 of 193, 0.5%) in fractures without clefts (Table 1). Cement leakage into the epidural vein was significantly more frequent in vertebrae without clefts compared with those with clefts ($p < 0.01$). On the other hand, disk leakage was significantly more frequent in vertebrae with clefts than in those without clefts ($p < 0.01$) (Table 1).

Symptomatic cement leakage developed in only four patients. One patient had radiculopathy caused by a large cement leak into the adjacent disk. Continuous pain for about 1 month at the puncture site caused by cement leakage into subcutaneous tissue through the needle track developed in three patients. No patients had symptoms from the epidural leakage.

Discussion

The presence or absence of clefts was diagnosed using not only preoperative radiography and MRI but also intraoperative fluoroscopy and the distribution of PMMA after injection on CT. The reason for these varying methods of detection was that the detection rate of clefts is low using preoperative diagnostic imaging alone, and in some cases clefts can be seen only after injecting PMMA [6, 17–19].

The amount of injected PMMA was greater for vertebral bodies with clefts compared with vertebral bodies without clefts, although there was no statistically significant difference in the volume of PMMA injected. In vacuum clefts containing gas or fluid, the level of resistance during cement injection was low because of low pressure inside the clefts, allowing a greater amount of cement into the cleft and increasing the cleft volume [5, 20].

There was no statistically significant difference in the incidence of cement leakage between vertebrae with clefts and those without clefts. These results agree with the report by Jung et al. [21], but Krauss et al. [15] reported that the incidence of leakage was lower for vertebral bodies with clefts than those without clefts. Krauss et al. indicated that cement leakage occurred in 18.2% (8 of 44) of clefts, whereas cement leakage occurred in 49.5% (53 of 107) of clefts in our series. The leakage rate of our series was significantly higher than in the series of Krauss et al. The mean cement volume injected by Krauss et al. was 3.1 mL, and the mean was 4.0 mL in our series. The cement volume injected was greater in our series than in that of Krauss et al. However, because Krauss et al. did not describe the end point of cement injection, the difference between their study and ours is not clear. Ha et al. [22] likewise reported that the incidence of leakage was higher for vertebral bodies with clefts compared with those without clefts.

Fig. 2—79-year-old woman with vertebral compression fracture with cleft of T12 due to osteoporosis. Sagittal CT image shows cement leakage into disk through part of destroyed endplate.

The incidence of leakage into the intervertebral disk was significantly higher for vertebral bodies with clefts than for vertebral bodies without clefts. The current study and the investigation by Jung et al. [21] were the only ones that have addressed the location of cement leakage from vertebral bodies with clefts, and our results agreed with the results obtained by Jung et al. The reason for cement leakage from vertebral bodies with clefts is

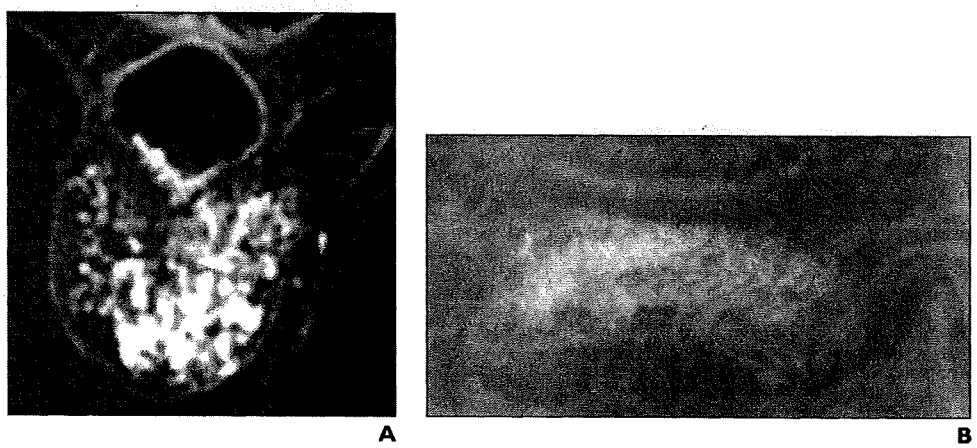

Fig. 3—73-year-old woman with vertebral compression fracture without cleft of T7 due to osteoporosis.
A, CT scan shows bone cement in epidural vein continuing to vertebral body. Cleft is not detected in fractured vertebral body.
B, Lateral spinal radiograph shows opaque cement interspersed through trabecular space.

primarily endplate damage, which is high for vertebral bodies with clefts, allowing cement to leak into the intervertebral disk via endplate damage. Furthermore, studies have reported that the vacuum phenomenon in vertebral bodies is associated with the vacuum phenomenon in the intervertebral disk [6, 23].

For vertebral bodies without clefts, leakage into the perivertebral veins occurred most commonly. The cancellous bone of vertebral bodies contains a rich internal vasculature that communicates with the epidural plexus and segmental veins. Moreover, we applied unilateral injection of cement in all cases. At the unilateral injection, the needle-tip is positioned on the midline of the vertebra. Basivertebral veins are primarily distributed in the midline portion of the vertebra. We think that a part of the cement was injected into the basivertebral veins and then leaked into the epidural veins. Therefore, cement injected into vertebral bodies readily leaks into veins through these passages [24].

Some limitations exist in the current study. First, the study was retrospective and only examined a small number of vertebral bodies. Second, all procedures were not performed by only one operator.

Injecting cement into clefts is easy, and fluoroscopy during injection shows that the height of vertebral bodies increases during injection. This tempts operators to inject more cement. However, our findings show that the incidence of cement leakage into the intervertebral disk is significantly higher in vertebral bodies with clefts, and leakage into the intervertebral disk may induce new compression fractures [11, 13, 14]. Caution must therefore be exercised during cement injection while keeping these points in mind.

In conclusion, there was no statistically significant difference in the incidence of cement leakage between vertebrae with clefts and those without clefts. However, cement leakage into the epidural vein was significantly more frequent in vertebrae without clefts compared with those with clefts, and leakage into the intervertebral disk was significantly more frequent in vertebrae with clefts than in those without clefts.

References

1. Kumpan W, Salomonowitz E, Seidl G, Wittich GR. The intravertebral vacuum phenomenon. *Skeletal Radiol* 1986; 15:444–447
2. Shih TT, Tsuang YH, Huang KM, Chen PQ, Su CT. Magnetic resonance imaging of vertebral compression fractures. *J Formos Med Assoc* 1996; 95:313–319
3. Benedek TG, Nicholas JJ. Delayed traumatic vertebral body compression fracture. Part II. Pathologic fractures. *Semin Arthritis Rheum* 1981; 10: 271–277
4. Resnick D. Vertebral body. In: Resnick D, ed. *Diagnosis of bone and joint disorders*, 3rd ed. Philadelphia, PA: Saunders, 1995:3527–3530
5. Maldague BE, Noel HM, Malghem JJ. The intravertebral vacuum cleft: a sign of ischemic vertebral collapse. *Radiology* 1978; 129:23–29
6. Lane JI, Maus TP, Wald JT, Thielen KR, Bobra S, Luetmer PH. Intravertebral clefts opacified during vertebroplasty: pathogenesis, technical implications, and prognostic significance. *AJNR* 2002; 23:1642–1646
7. Mirovsky Y, Anekstein Y, Shalmon E, Peer A. Vacuum clefts of the vertebral bodies. *AJNR* 2005; 26:1634–1640
8. Carlier RY, Gordji H, Mompoint DM, Vernhet N, Feydy A, Vallée C. Osteoporotic vertebral collapse: percutaneous vertebroplasty and local kyphosis correction. *Radiology* 2004; 233:891–898
9. Kim DY, Lee SH, Jang JS, Chung SK, Lee HY. Intravertebral vacuum phenomenon in osteoporotic compression fracture: report of 67 cases with quantitative evaluation of intravertebral instability. *J Neurosurg* 2004; 100[1 suppl spine]:24–31
10. Peh WC, Gelbart MS, Gilula LA, Peck DD. Percutaneous vertebroplasty: treatment of painful vertebral compression fracture with intraosseous vacuum phenomena. *AJR* 2003; 180:1411–1417
11. McKiernan F, Faciszewski T. Intravertebral clefts in osteoporotic vertebral compression fractures. *Arthritis Rheum* 2003; 48:1414–1419
12. Mathis JM. Vertebroplasty for vertebral fractures with intravertebral clefts. *AJNR* 2002; 23:1619–1620
13. Lin EP, Ekholm S, Hiwatashi A, Westesson PL. Vertebroplasty: cement leakage into the disc increases the risk of new fracture of adjacent vertebral body. *AJNR* 2004; 25:175–180
14. Komemushi A, Tanigawa N, Kariya S, et al. Percutaneous vertebroplasty for osteoporotic compression fracture: multivariate study of predictors of new vertebral body fracture. *Cardiovasc Intervent Radiol* 2006; 29:580–585
15. Krauss M, Hirschfelder H, Tomandl B, Lichti G, Bär I. Kyphosis reduction and the rate of cement leaks after vertebroplasty of intravertebral clefts. *Eur Radiol* 2006; 16:1015–1021
16. Theodorou DJ, Theodorou SJ, Duncan TD, Garfin SR, Wong WH. Percutaneous balloon kyphoplasty for the correction of spinal deformity in painful vertebral body compression fractures. *Clin Imaging* 2002; 26:1–5
17. Garfin SR, Reilley MA. Minimally invasive treatment of osteoporotic vertebral body compression fractures. *Spine J* 2002; 2:76–80
18. Trout AT, Kallmes DF, Lane JI, Layton KF, Marx WF. Subsequent vertebral fractures after vertebroplasty: association with intraosseous clefts. *AJNR* 2006; 27:1586–1591
19. Wiggins MC, Sehizadeh M, Pilgram TK, Gilula LA. Importance of intravertebral fracture clefts in vertebroplasty outcome. *AJR* 2007; 188:634–640
20. Golimbu C, Firooznia H, Rafii M. The intravertebral vacuum sign. *Spine* 1986; 11:1040–1043
21. Jung JY, Lee MH, Ahn JM. Leakage of polymethylmethacrylate in percutaneous vertebroplasty: comparison of osteoporotic vertebral compression fractures with and without an intravertebral vacuum cleft. *J Comput Assist Tomogr* 2006; 30:501–506
22. Ha KY, Lee JS, Kim KW, Chon JS. Percutaneous vertebroplasty for vertebral compression fractures with and without intravertebral clefts. *J Bone Joint Surg Br* 2006; 88:629–633
23. Lafforgue P, Chagnaud C, Daumen-Legre V, Daver L, Kasbarian M, Acquaviva PC. Intravertebral vacuum phenomenon ("vertebral osteonecrosis"): migration of intradiscal gas in a fractured vertebral body. *Spine* 1997; 22:1885–1891
24. Groen RJM, du Toit DF, Phillips FM, et al. Anatomical and pathological considerations in percutaneous vertebroplasty and kyphoplasty. *Spine* 2004; 29:1465–1471

Cardiovasc Intervent Radiol (2009) 32:1028–1032
DOI 10.1007/s00270-009-9622-7

LABORATORY INVESTIGATION

Mechanical Characteristics of Composite Knitted Stents

Takanori Tokuda · Yuzo Shomura · Noboru Tanigawa · Shuji Kariya · Atsushi Komemushi · Hiroyuki Kojima · Satoshi Sawada

Received: 11 October 2008 / Accepted: 19 May 2009 / Published online: 9 June 2009

Abstract We used metal wires and fibers to fabricate a composite knitted stent and then compare the mechanical characteristics of this stent with those of a pure metallic stent of the same construction in order to develop a stent that offers a comparable degree of expandability as metallic stents but can be used for highly curved lesions that cannot be treated using metallic stents. We fabricated two types of composite knitted stent (N–Z stents), using nitinol wire with a diameter of 0.12 mm and polyparaphenylene-benzobisoxazole (PBO) multifilament fiber (Zyron AS; Toyobo, Osaka, Japan). Stents were knitted into a cylindrical shape using the same textile pattern as a Strecker stent. Two loop lengths (L) of nitinol wire were used in the N–Z stents: L = 1.84 mm (N–Z stent L = 1.84) and L = 2.08 mm (N–Z stent L = 2.08). For the sake of comparison, we fabricated a metallic stent of nitinol using the same textile pattern (N–N stent L = 1.92). We applied a radial compression force diametrically to each stent and applied a bending force diametrically at the free end of a stent with one end fixed in order to evaluate the relationship between stent elasticity and load values. In addition, we macroscopically evaluated the generation of kinks when the stent was bent 180°. The radial compressive force when the stent diameter was reduced by 53% was 6.44 N in the case of N–Z stent L = 1.84, 6.14 N in the case of N–Z stent L = 2.08, and 4.96 N in the case of N–N stent L = 1.92 mm. The composite stent had a radial compressive force higher than that of a metallic stent. The restoring force to longitudinal direction at a 90° bending angle was 0.005 N for N–Z stent L = 1.84, 0.003 N for N–Z stent L = 2.08, and 0.034 N for N–N stent L = 1.92. The restoring force of the composite stent was significantly lower. Finally, the composite stent generated no definitive kinks at a bending angle of 180°, regardless of loop length. However, the N–N stent clearly produced kinks, causing blockage of the inner cavity. In conclusion, the use of a metal and fiber composite in the construction of a knitted stent ensures an expansion performance comparable to that of metallic stents, while providing better kink resistance.

Keywords Composite stent · Fiber · Radial force · Restoring force · Kink

T. Tokuda (✉) · Y. Shomura · N. Tanigawa · S. Kariya · H. Kojima · S. Sawada
Department of Radiology, Kansai Medical University Hirakata Hospital, 2-3-1 Shinmachi, Hirakata, Osaka 573-1191, Japan
e-mail: tkdtknr@gmail.com

A. Komemushi
Department of Radiology, Kansai Medical University Takii Hospital, 10-15 Humizonotyou, Moriguchi, Osaka 570-8506, Japan

Introduction

Metallic stents are made of materials such as nitinol and stainless steel. Their mechanical properties are mainly regulated by stent mesh design, properties of the metal, wall thickness, and radius. When the wall thickness and radius of some stents are comparable, stents that have a high degree of expandability tend to have a high degree of restoring force against bending deformation. Focusing on hollow organs that bend highly expandable stents, the restoring force generated during bending deformation results in excessive surface pressure being applied to tissue, and this can cause ulceration and tissue perforation [1]. In addition, during high-degree bending deformation, adjacent struts make contact and cause kinks, as they deform in a manner that allows them to protrude inwardly [2]. To resolve these

disadvantages of metallic stents, we fabricated composite knitted stents that combine two types of material, each having a different bending stiffness. With conventional stents used for the intestinal tract, biliary system, and vessels in joints, problems exist with patency and antikink properties, and we believe that the stent in the present study may be useful for stenting in such areas. Piquet et al. [3] and Hagen et al. [4] reported metal–fiber composite stents, but no studies assessing mechanical characteristics have been reported. The purpose of this study is to evaluate the mechanical properties of composite material stents fabricated by combining metallic and polymeric fibers.

Materials and Methods

Construction of Composite Material Stents

The materials used for the stents were nitinol wire with a diameter of 0.12 mm and polypara-phenylene-benzobisoxazole (PBO) multifilament fiber (ZYRON AS; Toyobo, Osaka, Japan) with a diameter of 0.18 mm. When achieving both expandability and restoring force with composite stents, shape memory treatment by heating nitinol is essential. PBO is a fibrous material but can withstand nitinol heat treatment. We knitted these in the same textile pattern (N–Z stent) (Fig. 1) as that of a Strecker stent [5].

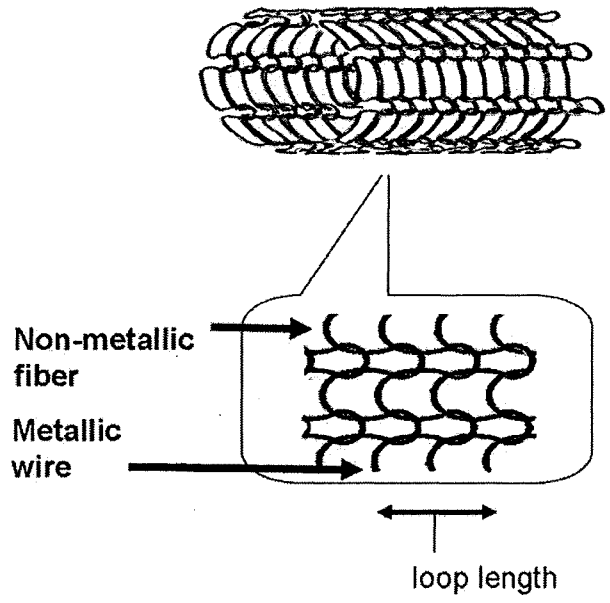

Fig. 1 Composite knitted stent. Nitinol wire and PBO fiber are alternately knitted. After being removed from the anchor, the composite stent is constricted longitudinally. We defined the distance of nitinol wires of composite stents after removal from the anchor as the loop length (L)

As composite stents are knitted with fiber materials under stretched conditions, when the anchor, which is a part of the knitting machine, is released, the length of the nitinol loops shrinks. Because stent expandability can be regulated by the loop length of the metallic wire during periods of no load, we defined the loop length of the no-load nitinol wire loop, L, as the loop length of the stent and used a 50× microscope (DS-3US; Magica, Osaka, Japan) to take actual measurements. We altered the knitting conditions and fabricated two types of composite knitted stents: an L = 1.84 mm N–Z stent (N–Z stent L = 1.84) and an L = 2.08 mm N–Z stent (N–Z stent L = 2.08). For the sake of comparison, we also fabricated an L = 1.92 mm metallic stent using nitinol alone (N–N stent L = 1.92).

The three trials fabricated stents were 15 mm in diameter and 80 mm long. After knitting, we heated the stents at 400°C for 30 min as a shape memory treatment for the nitinol alloy. Taking into account the balance between reduced PBO strength due to heating and the shape–memory properties of nitinol, a temperature of 400°C was selected.

Mechanical Strength of the Stent

With regard to the mechanical strength of the stent, we evaluated the following three items.

Radial Compressive Force

In stenting for hollow organ stenosis, we consider that patency >50% of the luminal diameter can often be achieved after stenting. As an indicator for assessing expandability after placing a stent in the body, the actual measurement range was set at compression until 53%. Even with 100% compression, however, the present stent was not deformed or destroyed. We installed two metal plates in a universal testing machine (RTC-1350A; Orientec Co., Ltd, Tokyo) and set the stent between the upper and the lower metallic plates. We lowered the upper metal plate until the stent diameter was 7 mm (47% of its original diameter) and used that as the measurement starting point. We moved the upper metal plate upward at a rate of 5 mm per minute to release compression. We then successively measured the relationship between stent distortion and load value by means of an autograph connected to the upper metal plate. After the stent reached its no-load point, we lowered the upper metal plate at a rate of 5 mm per minute and compressed the stent until reaching the measurement starting point. We considered this to be one cycle. We took an average of two cycles to measure the stent's radial compressive force [6] (Fig. 2).

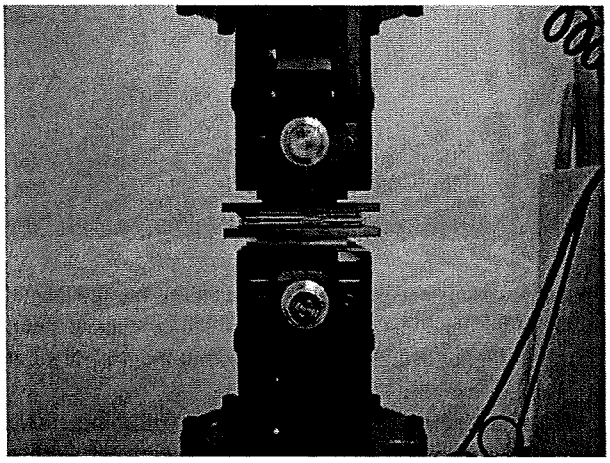

Fig. 2 Radial compressive force was measured using a universal testing machine (RTC-1350A; Orientec Co., Ltd, Tokyo)

Restoring Force

We inserted a mandrel 4 cm into one end of the stent and fixed the other end of the stent in place. We then attached a force gauge (DS2; Imada, Aichi, Japan) diametrically to the free end of the stent and applied external force through the gauge until the stent bent 90°. With the stent bent 90°, we measured the load value displayed on the force gauge. We took three measurements and took the average of these as the restoring force (Fig. 3).

Kink Resistance Performance

We inserted mandrels through both ends of the stent for a length of 2 cm and fixed both ends of the stent in place. We then bent the stent 180° until the mandrels became parallel.

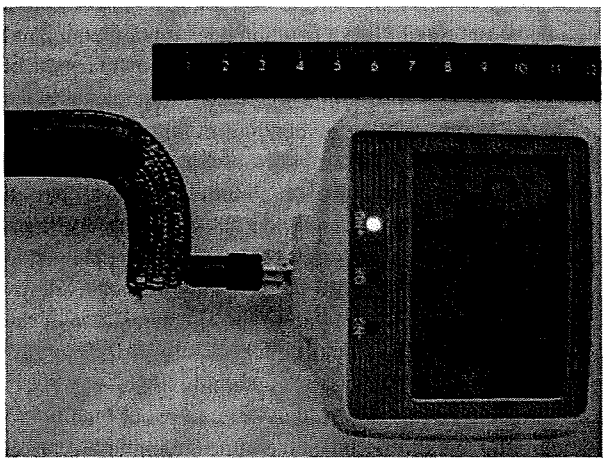

Fig. 3 Restoring force with the stent bent 90° was measured using a force gauge (DS2; Imada, Aichi, Japan)

Under these conditions, we visually assessed the kinking condition in the center of the stent (Fig. 4).

Results

Radial Compressive Force

The radial compressive forces of the stents with a compression load up to 47% of the diameter in the case of N–Z stent L = 1.84, N–Z stent L = 2.08, and N–N stent L = 1.92 increased in a curved line. The radial compressive force when each stent was compressed 9 mm (47% diameter reduction) was 6.44 N for N–Z stent L = 1.84 and 6.14 N for N–Z stent L = 2.08. The restoring force increased as the loop length of the metal became shorter and the density of the knit increased. In addition, the restoring force of N–N stent L = 1.92 was 4.96 N (Figs. 5, 6, 7). In other words, compared with the metallic stent, the composite stents showed a greater restoring force at the same metal knit density.

Restoring Force

Restoring forces when the stents were bent 90° were 0.005 N for N–Z stent L = 1.84, 0.003 N for N–Z stent L = 2.08, and 0.034 N for N–N stent L = 1.92.

Kink Resistance Performance

With N–N stent L = 1.92, we found an increase in kinking at restoring angles of $\geq$60°. With N–Z stent L = 1.84 and N–Z stent L = 2.08, we found a slight reduction in stent diameter when bending stents 100° or more, but at that level the diameter remained within 5% of the full diameter, irrespective of the knit density. Furthermore, we confirmed macroscopically that bending up to 150° did not produce any kinks.

Discussion

In this study, we fabricated composite knitted stents using nitinol and PBO fiber. We then compared the structural characteristics of these stents with those of a knitted metallic stent of the same construction.

At compression to 47% of its diameter, the radial compressive force of the composite knitted stent indicated a load value that increased in a curved line to the amount of compression. Comparison of composite knitted stents showed that shorter loop lengths had higher load values. Wright et al. reported that for metal stents, the larger the number of vents, the greater the expandability [7]. This

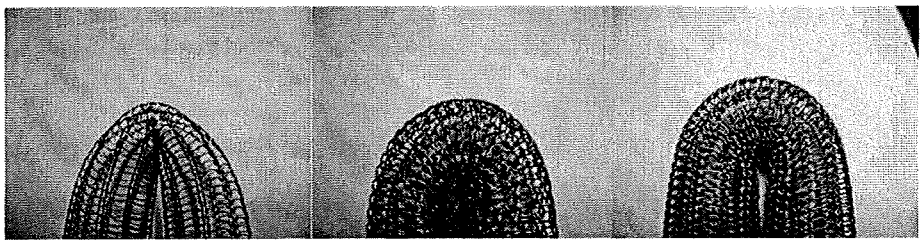

Fig. 4 Compared to the N–Z stent (*center* and *right*), the N–N stent (*left*) shows obvious kinking at bending angles of 180°

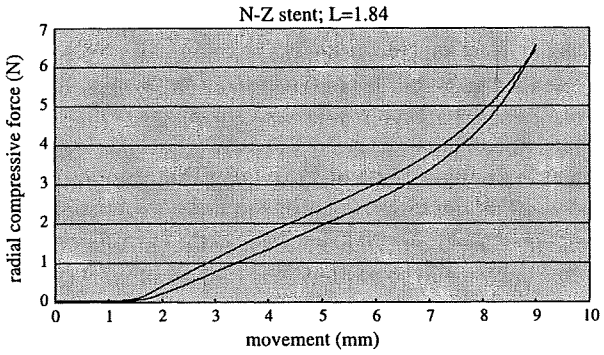

Fig. 5 Relationship between movement of upper metallic plate and radial compressive force of N–Z stent; L = 1.84

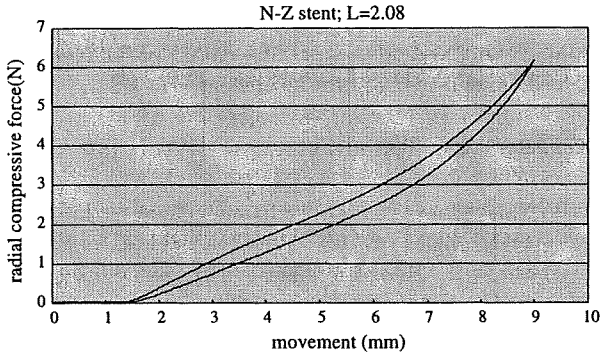

Fig. 6 Relationship between movement of upper metallic plate and radial compressive force of N–Z stent; L = 2.08

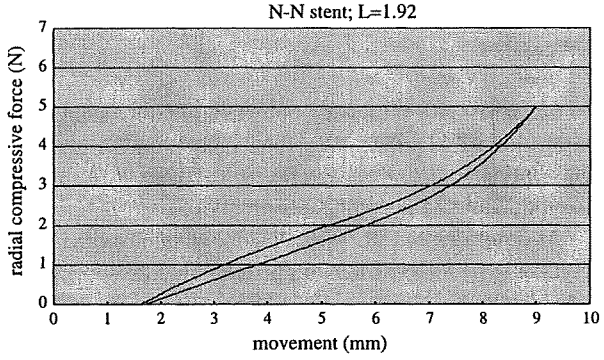

Fig. 7 Relationship between movement of upper metallic plate and radial compressive force of N–N stent; L = 1.92

tendency was also seen with hybrid material knitted stents. On the other hand, N–Z stent L = 2.08, a composite stent, showed a higher radial compressive force than N–N stent L = 1.92, a metallic stent.

We think the reason for this high radial compressive force response despite the longer loop length is because fibers knitted with nitinol prevent deformation of metallic wire. Fibers have tolerance for bending but can have longitudinal resistance for elasticity. As a result, a high radial compressive force is maintained despite the larger loop length.

With regard to restoring force, compared to a metallic stent with a similar knit density, the composite knitted stent showed lower values, and no kinks were seen macroscopically. Mori et al. investigated the mechanisms of stent kink generation using finite-element method analysis and found that the interference between struts reduces flexibility and leads to kinking [2]. In the case of a composite knitted stent, a fiber loop is adjacent to a metal loop. Even if these interfere during bending deformation, the fiber loop deforms easily and generates no restoring force because the fiber has almost no bending stiffness, therefore the main cause of restoring force during bending deformation is the recoil force related to the curvature of the metal wire. As a result, we see a low overall restoring force.

The composite stents fabricated here had a general knit weave construction, similar to that of the Strecker stent and Ultraflex stent. The knit weave construction reportedly has a high degree of flexibility in bending deformation compared with other types of knitting [8]. However, as in the results of this experiment, using a single metal construction clearly led to kinks at high degrees of bending deformation and the restoring force was also high. Solving these problems involves designing a wide loop alignment interval, but an alignment interval that is too wide will not allow for practical expandability. A composite knitted stent is believed to have mechanical properties that cannot be achieved by metallic stent construction due to the characteristics of the fiber components. We think it could be useful for the gastrointestinal tract, biliary tract, and highly flexed vessel.

Limitations of this experiment were, first, our inability to compare the metallic stents and composite knitted stents at the same loop length. This is because releasing the anchor when knitting the composite stent caused the multifilament

fibers to contract, which then caused the nitinol loop length to shrink. To fabricate a stent at the designated loop length requires clarifying the relationship between the knitting conditions and the rate of shrinkage. Second, the safety of PBO in the body has not been investigated. The possibility of foreign body reactions in the body will need to be assessed using animal studies in future.

Conclusions drawn from this study are as follows. Compared with a metal stent of the same design, a composite knitted stent comprising metal and fiber materials allows for a high radial compressive force and a low restoring force. In addition, compared with a metallic stent, the use of composite materials provides excellent resistance to kinking.

References

1. Fransen GA, Desgranges P, Laheij RJ, Harris PL, Becquemin JP (2003) Frequency, predictive factors, and consequences of stent-graft kink following endovascular AAA repair. J Endovasc Ther 10:913–918
2. Mori K, Saito T (2005) Effects of stent structure on stent flexibility measurements. Ann Biomed Eng 33:733–742
3. Piquet P, Rolland PH, Bartoli JM et al (1994) Tantalum–Dacron coknit stent for endovascular treatment of aortic aneurysms: a preliminary experimental study. Vasc Surg 19:698–706
4. Hagen B, Harnoss BM, Trabhardt S, Ladeburg M, Fuhrmann H, Franck C (1993) Self-expandable macroporous nitinol stents for transfemoral exclusion of aortic aneurysms in dogs: preliminary results. Cardiovasc Intervent Radiol 16:339–342
5. Strecker EP, Liermann D, Barth KH, Wolf HRD, Freudenberg N (1990) Expandable tubular stents for treatment of arterial occlusive diseases: experimental and clinical results. Radiology 175:97–102
6. Flueckiger F, Sternthal H, Klein GE, Aschauer M, Szolar D, Kleinhappl G (1994) Strength, elasticity, and plasticity of expandable metal stents: in vitro studies with three types of stress. J Vasc Interv Radiol 5:745–750
7. Wright KC, Wallace S, Charnsangavej C, Carrasco CH, Gianturco C (1985) Percutaneous endovascular stent; an experimental evaluation. Radiology 156:69–72
8. Okuda Y, Sawada S, Morioka N et al (1995) Physical properties of Strecker stents. Nippon Igaku Hoshasen Gakkai Zasshi 55(3):129–132

Jpn J Radiol (2009) 27:176–179
DOI 10.1007/s11604-009-0316-5

CASE REPORT

Percutaneous translumbar inferior vena cava cannulation under computed tomography guidance

Shuji Kariya · Noboru Tanigawa · Hiroyuki Kojima
Atsushi Komemushi · Yuzo Shomura
Sang Kil Ha-Kawa · Takanori Tokuda · Minoru Kamata
Satoshi Sawada

Received: September 23, 2008 / Accepted: February 3, 2009

Abstract Percutaneous translumbar inferior vena cava (IVC) cannulation is an alternative approach for central venous catheterization, but there have been sporadic reports of puncture-related complications. To avoid complications during IVC puncture, percutaneous translumbar IVC cannulation was performed under computed tomography (CT) guidance in addition to fluoroscopy in two patients. To perform chemotherapy for recurrent breast cancer, we planned subcutaneous port catheter placement for central venous access. Under CT guidance, the direction and insertion distance of a long elastor needle were adjusted, and the IVC was punctured at the level of the third lumbar vertebra while taking care to avoid the right urinary tract. A guidewire was inserted through the long elastor needle, and a catheter was placed over the guidewire. It was possible to perform central venous catheterization by percutaneous translumbar inferior vena cava cannulation under CT guidance.

Key words Translumbar · Vena cava · Catheter · Vascular access · Percutaneous

S. Kariya (✉) · N. Tanigawa · H. Kojima · A. Komemushi · Y. Shomura · S.K. Ha-Kawa · T. Tokuda · M. Kamata · S. Sawada
Department of Radiology, Kansai Medical University, 2-3-1 Shinmachi, Hirakata 573-1192, Japan
Tel. +81-72-804-0101; Fax +81-72-804-2865
e-mail: shuuji@ops.dti.ne.jp

Introduction

For central venous catheterization, the subclavian vein, internal jugular vein, femoral vein, or upper extremity peripheral vein is generally targeted. However, when these vascular accesses are unavailable, it is necessary to consider placing a percutaneous inferior vena cava (IVC) catheter by translumbar cannulation, transhepatic cannulation, or transhepatic vein cannulation as an alternative.[1–14] To avoid complications during IVC cannulation, we performed percutaneous translumbar IVC cannulation under computed tomography (CT) guidance for two patients.

Case reports

Case 1

The patient was a 60-year-old woman with a height of 151 cm and a body weight of 45 kg. She underwent left mastectomy for left breast cancer 8 years previously and had since repeatedly undergone chemotherapy and radiotherapy for bone, skin, lymph node, and liver metastases. Here, we planned subcutaneous port catheter placement for central venous access to perform chemotherapy. The patient had an invasive 12-cm tumor in the left anterior chest wall. The skin around the tumor was red, reaching the right anterior chest wall. The tumor in the left anterior chest wall reached the anterior mediastinum and was located in the vicinity of the area where the left and right brachiocephalic veins merged. Subsequently, cervical, clavicular, and upper extremity approaches were ruled out; and percutaneous translumbar IVC cannulation was selected.

Case 2

The patient was a 58-year-old woman with a height of 159 cm and a body weight of 50 kg. The patient underwent left mastectomy for right breast cancer 3 years previously and had since repeatedly undergone chemotherapy and radiotherapy for bone, skin, lymph node, and liver metastases. Here, we planned subcutaneous port catheter placement for central venous access to perform chemotherapy. The patient had multiple skin metastases in the bilateral anterior chest wall and neck. Subsequently, cervical, clavicular, and upper extremity approaches were ruled out; and percutaneous translumbar IVC cannulation was selected.

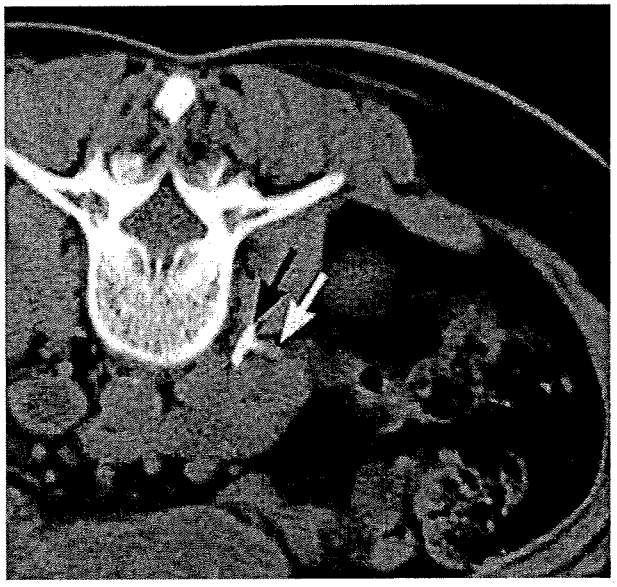

Fig. 1. Under computed tomography (CT) guidance, a 15-cm 21-gauge long elastor needle was inserted into the inferior vena cava (IVC) (*black arrow*) in a 60-year-old woman. After confirming the location of the right urinary tract (*white arrow*), caution was exercised to avoid it

Procedure

After obtaining informed consent, subcutaneous port catheter placement for central venous access was performed by percutaneous translumbar IVC cannulation in both patients.

The patient was placed in the prone position. During the procedure, electrocardiography (ECG), percutaneous oxygen saturation, and blood pressure were monitored. The maximal barrier precaution technique was employed. The procedure was performed under conscious sedation (hydroxyzine).

At the height of the iliac crest, local anesthesia was induced by injecting 1% lidocaine (Xylocaine; AstraZeneca, Osaka, Japan) 7 cm right of the dorsal midline; a 1-cm incision was then performed to serve as a temporary entry site. Under fluoroscopic guidance, a 10-cm 21-gauge needle was inserted through the temporary entry site into the right margin of the third lumbar vertebra to a depth of 8 cm to anesthetize the puncture pathway additionally. Next, a 15-cm 21-gauge long elastor needle (Medikit, Miyazaki, Japan) was inserted in the same direction to a depth of 8 cm. Then, while adjusting the direction and distance under CT guidance, the IVC was punctured at the level of the third lumbar vertebra. While advancing the needle, caution was exercised to avoid the right urinary tract in front of the iliopsoas muscle (Fig. 1). CT was performed four times in case 1 and six times in case 2 to puncture the IVC using the long elastor needle. After confirming that the tip of the long elastor needle was within the IVC, a 0.025-inch wire (fixed core wire guide Safe-T-J; Cook, Bloomington, IN, USA) was inserted through the outer cannula of the long elastor needle. The wire tip passed through the right atrium and was placed in the brachiocephalic vein. A 4F 25 cm long sheath introducer (Medikit) was inserted over the guidewire. After determining the location of the port reservoir (BardPort Titanium Low Profile; Bard, Salt Lake City, UT, USA), a subcutaneous pocket was prepared. The port was placed 4 cm dorsal to the right middle axillary line and 5 cm cranial to the 4F sheath introducer insertion site. Using the Tunneler (Bard), a tunnel was prepared from the subcutaneous pocket to the temporary entry site, and an indwelling 8F catheter (Groshong Catheter, Bard) was placed. After tunneling, a 0.035-inch wire (Amplatz Super Stiff; Boston Scientific, Natick, MA, USA) was inserted through the 4F angiosheath, and the tip of the wire was paced in the brachiocephalic vein. Using the wire, the 4F angiosheath was replaced with a 9F 25 cm long peel-off introducer (Medikit). The 8F catheter was passed through the peel-off introducer, and the introducer was then peeled away. The tip of the catheter was placed in the right atrium. The port was connected to the catheter and was then implanted in the subcutaneous pocket, and the wound was closed.

Abdominal radiography and contrast-enhanced CT were performed to check for complications (Figs. 2, 3) The contrast-enhanced CT was employed after placing the catheter in case 1 and before inserting the 9F 25 cm long peel-off introducer in case 2. The patient of case 1 was hospitalized for 2 days, and the patient of case 2 was hospitalized after the procedure continuously for chemotherapy. It was possible to perform chemotherapy using the port reservoir.

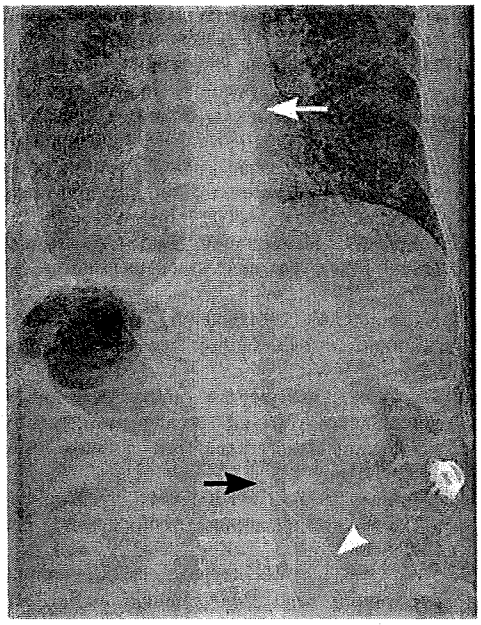

Fig. 2. Abdominal radiograph of a 60-year-old woman. The catheter tip was placed in the right atrium (*white arrow*). *Black arrow*, IVC cannulation. *White arrowhead*, temporary entry site

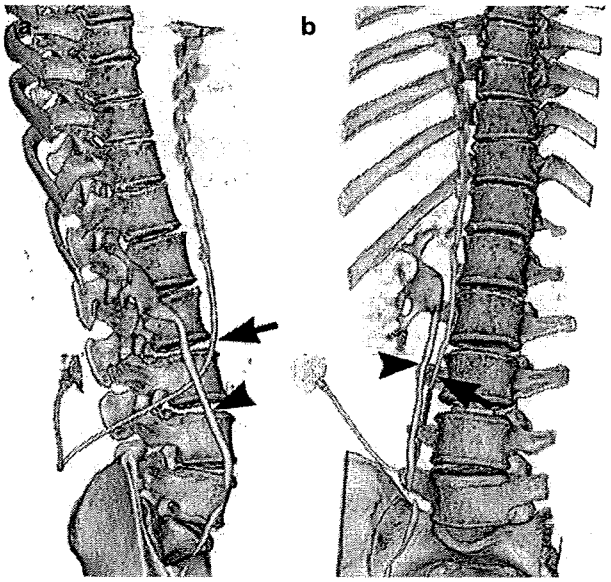

Fig. 3. Three-dimensional images reconstructed from contrast-enhanced CT scans following central venous catheterization by percutaneous translumbar IVC cannulation in a 60-year-old woman. **a** The catheter (*arrow*) and urinary tract (*arrowhead*) intersected at the level of the third lumbar vertebra. **b** The catheter (*arrow*) and urinary tract (*arrowhead*) were separated, confirmed by CT during cannulation

Discussion

When inserting a central venous catheter from the upper body, the subclavian vein, internal jugular vein, or peripheral brachial vein is used; but central vein stenosis or skin damage at the puncture site might prevent the selection of one of these veins. Although it is possible to insert a catheter from the femoral vein, several studies have found that central venous catheterization through the femoral vein should be performed only in emergencies or in children.[15,16] In addition, when involving the femoral vein, there is a risk for thrombosis in the iliac and femoral veins.[15,17] As alternative approaches to conventional cannulation, central venous catheter placement by translumbar cannulation, transhepatic cannulation, or transhepatic vein cannulation has been reported.[1–14] When cannulating the IVC using an alternative approach, studies have reported that translumbar cannulation should be used preferentially because it is associated with fewer complications than percutaneous transhepatic cannulation.[10,18,19] Translumbar cannulation was first reported by Kenney in 1985, and its use has been documented in a large number of cases with clinical results and complications in studies from the United States. [1,2,4–8,10–13]

The situations for which translumbar IVC cannulation has been selected are as follows.[20,21] First, traditional access sites other than the femoral vein cannot be used. Second, it is needed for long-term placement of a large-bore catheter used for access of infusion or dialysis even if the femoral vein approach can be used. Third, a central venous approach for interventional treatment is needed when the femoral vein approach cannot be used because of an occluded IVC, such as existence of the thrombosed IVC filter.

The incidence of late complications associated with central venous catheter access by percutaneous translumbar IVC cannulation is as follows: 0.24 episodes of infection per 100 catheter-days and 0.22 thrombosis-related catheter failures per 100 catheter-days, both which are comparable to those seen with conventional cannulation.[5,12] However, retroperitoneal hematoma, damaged renal artery branch, punctured aorta, punctured superior mesenteric vein, and damaged urinary tract have been reported as complications of central venous catheter placement by percutaneous translumbar IVC cannulation, and they are unique to translumbar cannulation.[6,13,22,23]

While conventional central venous cannulation is performed under echo guidance, translumbar cannulation is performed using radiopaque instruments such as guidewires, catheters, wire baskets, or intravascular snares as visual markers, thus resulting in the above-mentioned complications. With our method, the IVC was punctured using the interventional radiology (IVR)-CT system under fluoroscopic and CT guidance. Using

this method, it is possible to avoid accidentally damaging arteries, the urinary tract, and other organs that can be identified by CT. Particularly for cannulation under fluoroscopic guidance, it is difficult to avoid damaging the urinary tract, even if fluoroscopy is performed from two directions. When treating a damaged urinary tract, it may be necessary to place a catheter for a period of time; hence, it is clinically useful to avoid puncturing the urinary tract under CT guidance.[22,23] Contrast-enhanced CT for guidance when puncturing the IVC may be helpful for visualizing the urinary tract, artery, and IVC.

When placing the catheter through the iliopsoas muscle, CT cannot identify arteries vascularizing the iliopsoas muscle, but it can discover retroperitoneal hemorrhage at early stages during the procedure, thus enabling early therapy. According to Bennett et al., retroperitoneal hematoma was not discovered immediately after placement but was seen at 48 h after catheter placement due to flank pain and bruising, confirmed by CT.[13] Cazenave et al.[24] deduced a safe pathway for percutaneous translumbar IVC cannulation by CT and discussed the slope of the puncture needle under fluoroscopic guidance. This suggests that a safe pathway can be determined under CT guidance; however, to the best of our knowledge, there have been no clinical reports on CT-guided cannulation.

One disadvantage of our method is that IVR-CT is required for CT and fluoroscopic guidance. In addition, because CT has been performed several times to examine the area between the third lumbar vertebra and the iliac crest, the amount of radiation exposure to the patient might be greater.

In conclusion, it was possible to perform central venous catheterization by percutaneous translumbar IVC cannulation under CT guidance.

References

1. Kenney PR, Dorfman GS, Denny DF Jr. Percutaneous inferior vena cava cannulation for long-term parenteral nutrition. Surgery 1985;97:602–5.
2. Denny DF Jr, Dorfman GS, Greenwood LH, Horowitz NR, Morse SS. Translumbar inferior vena cava Hickman catheter placement for total parenteral nutrition. AJR Am J Roentgenol 1987;148:621–2.
3. Crummy AB, Carlson P, McDermott JC, Andrews D. Percutaneous transhepatic placement of a Hickman catheter. AJR Am J Roentgenol 1989;153:1317–8.
4. Denny DF Jr, Greenwood LH, Morse SS, Lee GK, Baquero J. Inferior vena cava: translumbar catheterization for central venous access. Radiology 1989;172:1013–4.
5. Haire WD, Lieberman RP, Lund GB, Wieczorek BM, Armitage JO, Kessinger A. Translumbar inferior vena cava catheters: safety and efficacy in peripheral blood stem cell transplantation. Transfusion 1990;30:511–5.
6. Lund GB, Lieberman RP, Haire WD, Martin VA, Kessinger A, Armitage JO. Translumbar inferior vena cava catheters for long-term venous access. Radiology 1990;174:31–5.
7. Cazenave FL, Glass-Royal MC, Teitelbaum GP, Zuurbier R, Zeman RK, Silverman PM. CT analysis of a safe approach for translumbar access to the aorta and inferior vena cava. AJR Am J Roentgenol 1991;156:395–6.
8. Haire WD, Lieberman RP, Lund GB, Kessinger A. Translumbar inferior vena cava catheters. Bone Marrow Transplant 1991;7:389–92.
9. Kaufman JA, Greenfield AJ, Fitzpatrick GF. Transhepatic cannulation of the inferior vena cava. J Vasc Interv Radiol 1991;2:331–4.
10. Azizkhan RG, Taylor LA, Jaques PF, Mauro MA, Lacey SR. Percutaneous translumbar and transhepatic inferior vena caval catheters for prolonged vascular access in children. J Pediatr Surg 1992;27:165–9.
11. Gupta A, Karak PK, Saddekni S. Translumbar inferior vena cava catheter for long-term hemodialysis. J Am Soc Nephrol 1995;5:2094–7.
12. Lund GB, Trerotola SO, Scheel PJ Jr. Percutaneous translumbar inferior vena cava cannulation for hemodialysis. Am J Kidney Dis 1995;25:732–7.
13. Bennett JD, Papadouris D, Rankin RN, McGloughlin RF, Kribs S, Kozak RI, et al. Percutaneous inferior vena caval approach for long-term central venous access. J Vasc Interv Radiol 1997;8:851–5.
14. Rodriguez-Cruz E, Bonilla M, Perez J. Percutaneous translumbar inferior vena cava catheter placement for long-term hemodialysis treatment. Pediatr Nephrol 2007;22:612–5.
15. Pippus KG, Giacomantonio JM, Gillis DA, Rees EP. Thrombotic complications of saphenous central venous lines. J Pediatr Surg 1994;29:1218–9.
16. Trottier SJ, Veremakis C, O'Brien J, Auer AI. Femoral deep vein thrombosis associated with central venous catheterization: results from a prospective, randomized trial. Crit Care Med 1995;23:52–9.
17. Zaleski GX, Funaki B, Lorenz JM, Garofalo RS, Moscatel MA, Rosenblum JD, et al. Experience with tunneled femoral hemodialysis catheters. AJR Am J Roentgenol 1999;72:493–6.
18. De Csepel J, Stanley P, Padua EM, Atkinson JB. Maintaining long-term central venous access by repetitive hepatic vein cannulation. J Pediatr Surg 1994;29:56–7.
19. Putnam SG 3rd, Ball D, Cohen GS. Transhepatic dialysis catheter tract embolization to close a venous-biliary-peritoneal fistula. J Vasc Interv Radiol 1998;9:149–51.
20. Brueck M, Bandorski D, Kramer W, Rauber K. Inferior vena cava approach to permanent pacemaker implantation. Pacing Clin Electrophysiol 2007;30:813–6.
21. Wible BC, Hieb R, Halum R, Rilling W. IVC stent deployment via translumbar approach. J Vasc Interv Radiol 2005;16:733–6.
22. DiMasi MH, Reid SK, Pagan-Marin H, Kirchner TM. Migration of translumbar inferior vena cava catheter into the right ureter. AJR Am J Roentgenol 1997;169:1753–4.
23. Elduayen B, Martinez-Cuesta A, Vivas I, Delgado C, Pueyo JC, Bilbao JI. Central venous catheter placement in the inferior vena cava via the direct translumbar approach. Eur Radiol 2000;10:450–4.
24. Cazenave FL, Glass-Royal MC, Teitelbaum GP, Zuurbier R, Zeman RK, Silverman PM. CT analysis of a safe approach for translumbar access to the aorta and inferior vena cava. AJR Am J Roentgenol 1991;156:395–6.